Passive Properties of Cr12Ni3Co12Mo4W Ultra-High-Strength Martensitic Stainless Steel

Huiyan Li[1], Shiwen Zou[2], Chaofang Dong[1,*] , Kui Xiao[1], Xiaogang Li[1], Ping Zhong[3]

[1] Corrosion and Protection Center, Key Laboratory for Corrosion and Protection (MOE), University of Science and Technology Beijing, Beijing 100083, China
[2] Aerospace Research Institute of Materials &Processing Technology, Beijing, 100076, China
[3] Beijing Institute of Aeronautical Materials, Beijing 100095, China
[*]E-mail: cfdong@ustb.edu.cn

The passive properties of the Cr12Ni3Co12Mo4W ultra-high-strength martensitic stainless steel were investigated by surface analysis techniques and electrochemical measurements. The potentiodynamic polarization curves exhibited a wide passivity region, which indicated that the ultra-high-strength martensitic stainless steel exhibited excellent electrochemical characteristics in 0.1 M Na_2SO_4 solution (pH = 3). The thickness of the passive films increased from 0.7 nm to 5.2 nm with the increase of film formation potential. The passive films formed at different potentials exhibited n- and p-type semiconductor behaviors. The passive films formed at more positive potentials were more stable, with lower oxygen vacancy concentrations than those formed at lower potentials. The films formed at anodic potentials primarily comprised FeO, Fe_3O_4, Fe_2O_3, Cr_2O_3, $Cr(OH)_3$, NiO and MoO_3. The passive films formed at anodic potentials were predominantly composed of Fe oxides, whereas those formed at cathodic potentials were primarily composed of oxides and hydroxides of Cr. The contribution of alloy element Ni to the passivity performance of the steel was larger than that of Mo. During the pitting corrosion, the passive films remarkably increased the pitting potential.

1. INTRODUCTION

Ultra-high-strength stainless steels are widely used in tissue engineering, aircraft devices, and ocean equipment because of their combination of excellent specific strength and durability [1-4]. In the past, a key impediment to the application of stainless steels was the requirement of high strength; in response, heat-treatment processes and alloy compositions were adjusted to produce ultra-high-

strength stainless steels. The development of martensitic steels with high strength and hardness was considered to solve the strength problem. Martensitic stainless steels are extensively used in applications requiring both high mechanical strength and high corrosion resistance [5-8]. The Cr12Ni3Co12Mo4W ultra-high-strength martensitic stainless steels (UHSMSSs) studied in this paper were designed as an aircraft undercarriage material with 2000MPa strength.

With the expanded application of martensitic stainless steels, a new problem has arisen. The high distortion energy of martensite ensures its high hardness and strength; however, higher distortion energy also results in higher activity, which facilitates corrosion. The corrosion resistance of stainless steels is well known to depend on the passive film formation and breakdown behaviors that occur during exposure to various corrosive environments [9-12]. The chromium content in UHSMSS is greater than 12%, and passivity and pitting are the key issues affecting corrosion resistance. Previous reports related to passive films of austenitic stainless steels are mainly focused on the film's thickness, structure, and composition [13-15]. The passive films of some austenitic stainless steels, such as 304 and 316 stainless steels, comprise an inner layer of Cr_2O_3 and an outer layer of Fe_3O_4 [16-17]. The proportion of Fe/Cr in the passive film plays a key role in determining the corrosion resistance. PDM theory is generally used to analyze the kinetics of passive film growth and defect diffusivity on the basis of Mott-Schottky plots and electrochemical impedance spectroscopy (EIS) [18-19].

To the best of our knowledge, little work concerning passive film formation on UHSMSS has been reported. In our previous studies, we investigated the correlations among the heat-treatment process, microstructure, alloying elements, mechanical properties, and corrosion behavior of the UHSMSS [20-21]. Nevertheless, a better understanding of the passive properties of this steel is critical for studying its corrosion resistance and for providing reference data needed for material design. Accordingly, in this study, the structure, composition, and defect diffusivity of the passive film formed on the Cr12Ni3Co12Mo4W UHSMSS at different formation potentials are studied by X-ray diffraction and electrochemical methods.

2. EXPERIMENTS

2.1 Experimental material

The Cr12Ni3Co12Mo4W UHSMSS with the chemical composition listed in Table 1 was used in the experiments. UHSMSS was heated at 1080°C for austenitization, oil quenched to room temperature, cooled for 1 h at -73°C to transform the retained austenite, and finally tempered at 600°C for 4 h.

Table 1. Chemical composition of the Cr12Ni3Co12Mo4W UHSMSS (wt.%)

Element	C	Cr	Co	Mo	Ni	W	V	Ti	Si	Mn
Wt.%	0.089	12.41	12.3	4.43	2.59	0.98	0.24	<0.005	0.053	<0.10

The Cr12Ni3Co12Mo4W UHSMSS specimens were cut into 10 mm × 10 mm × 5 mm samples, each with a working surface area of 1cm^2; the samples were then grounded, polished, and etched with (HF: HCl: H$_2$O = 4:4:92) solution. A stereological microscope (KEYENCE VHX-2000C) was used to observe the microstructure of the steel. To further reveal the microstructure, the specimens were thinned using a Gatan 691 precision ion polishing system using argon ions at 5 kV and were then observed under a JEM-2100F high-resolution transmission electron microscope operated at 200 keV. The microstructure of UHSMSS (Fig. 1) comprises lath/plant martensite, some retained austenite and carbides distributed within the matrix and at the boundaries.
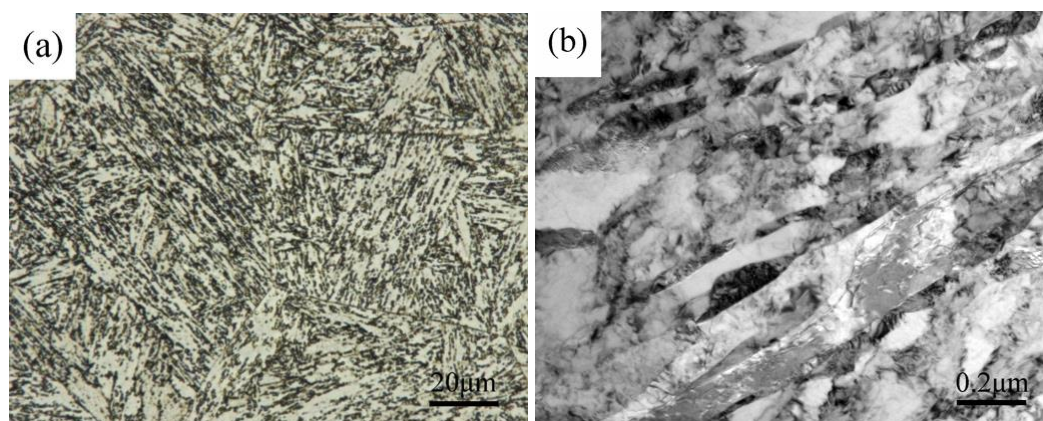
Figure 1. Microstructure (a) and TEM image (b) of the Cr12Ni3Co12Mo4W UHSMSS

2.2 Electrochemical tests

The electrochemical samples were embedded in epoxy resin, leaving a working area of 1 cm^2; they were then grounded to 1000 grit and cleaned with ethanol and deionized water before the electrochemical tests. The electrochemical measurements were performed at room temperature (~25°C)in a conventional three-electrode cell using a M370 advanced electrochemical system. UHSMSS was used as the working electrode, a platinum sheet was used as the counter electrode, and all potentials were measured against a saturated calomel electrode (SCE) connected to the cell via a Luggin probe. The experimental electrolyte was 0.1 M Na$_2$SO$_4$ solution (pH = 3) prepared using reagent-grade Na$_2$SO$_4$ and deionized water.

Before the electrochemical measurements, the working electrodes were initially reduced potentiostatically at -1.2 V$_{SCE}$ for 3 min to reduce the air-formed oxide film on the specimen surface. EIS measurements were performed using an applied potential amplitude of 10 mV at the open-circuit potential (OCP) in the frequency range from 100 kHz to 10 mHz. For Mott-Schottky measurements, the potential sweeping rate was 25 mV/s at a frequency of 1 kHz. The polarization curves were measured potentiodynamically from -0.3 V (vs. corrosion potential E_{corr}) to 1.8 V$_{SCE}$ at a scanning rate of 0.5 mV/s.

2.3 Surface analysis

The chemical composition of the surface passive films formed on the Cr12Ni3Co12Mo4W UHSMSS obtained by immersion in 0.1 M Na_2SO_4 solution (pH = 3) at -0.45 V_{SCE}, OCP, 0.1 V_{SCE} and 0.6 V_{SCE} for 5 h was examined by X-ray photoelectron spectroscopy (XPS) on a spectrometer (Fisons Escalab 250) equipped with an Al Kα X-ray source (hv = 1486.6 eV) operated at 15 kV and 20 mA. The binding-energy scale was calibrated on the basis of the C 1s peak at 284.5 eV. Spectra of Fe $2p_{3/2}$, Cr $2p_{3/2}$, Ni $2p_{3/2}$, Mo 3d, and O 1s were recorded. The spectra were analyzed using the parameters of standard peaks.

The surface morphology of the passive film on UHSMSS formed at OCP for 2 h and the fresh surface after erosion was observed using atomic force microscopy (AFM, Bruker multiMode 8.0) in tapping mode.

The surface morphology of UHSMSS after immersion in 0.1 M Na_2SO_4 solution (pH = 3) at 1.4 V_{SCE} for 5 min was observed using an FEI Quanta250 environmental scanning electron microscope (SEM).

3. RESULTS AND DISCUSSION

3.1 Passivation performance of the Cr12Ni3Co12Mo4W UHSMSS

The potentiodynamic polarization curve of the Cr12Ni3Co12Mo4W UHSMSS measured in 0.1 M Na_2SO_4 solution (pH = 3) is shown in Fig. 2. The SEM morphology of the UHSMSS after immersion in 0.1 M Na_2SO_4 solution (pH = 3) at 1.4 V_{SCE} for 5 min is also shown in Fig. 2. When the potential was too positive, the pitting occurred on the surface of the steel.
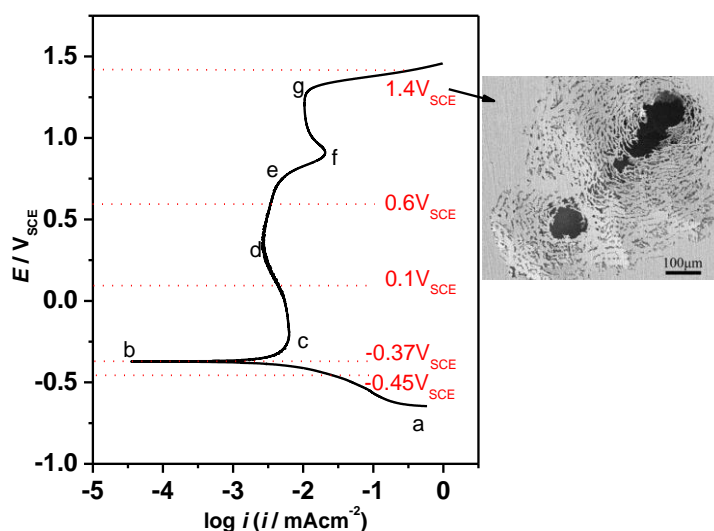
**Figure 2.** Polarization curve of the Cr12Ni3Co12Mo4W UHSMSS in 0.1 M Na_2SO_4 solution (pH = 3)
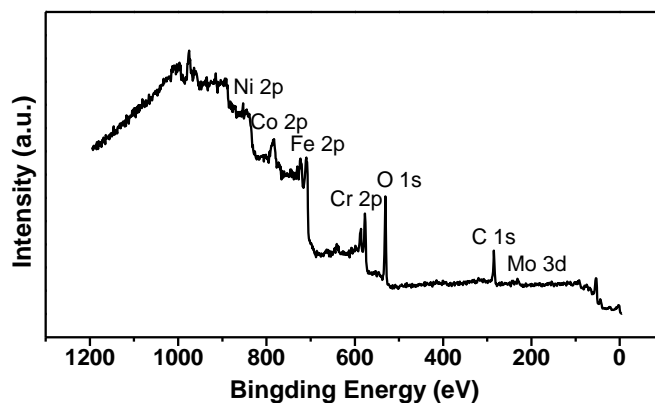
Figure 3. XPS survey spectra for passive film formed on the Cr12Ni3Co12Mo4W UHSMSS in 0.1 M Na$_2$SO$_4$ solution (pH = 3) at OCP for 2 h

The steel exhibits typical anodic polarization. When the potential was more negative than -0.37 V$_{SCE}$ (point b in Fig. 3), UHSMSS underwent a cathodic process. From point b toward positive potentials, the current increased with the potential, approaching point c (-0.25 V$_{SCE}$, -2.2 mAcm^{-2}), where UHSMSS entered an active region. UHSMSS was in an active-passive region from point c to point d, where the passivating current density decreased and then entered a passive region from point d to point e. When the potential was more positive than 1.0 V$_{SCE}$, UHSMSS underwent a transpassive process [19], where the current density sharply increased, accompanied by the oxygen evolution reaction on the passive film surface. This passive potential region is larger than that of 304 stainless steel in acid solution [16]. The corrosion potential, passivity current density, and corrosion current density indicate that the corrosion resistance of the Cr12Ni3Co12Mo4W UHSMSS in Na$_2$SO$_4$ solution closely matches that of the Cr9Ni5MoCo14 UHSMSS [12]. The adjustment of the alloy elemental composition of these two UHSMSSs improves their mechanical strength while maintaining their excellent corrosion resistance.

3.2 Surface morphology of passive films

As seen from Fig.2, UHSMSS exhibits excellent passivation properties in 0.1 M Na$_2$SO$_4$ solution (pH = 3) for the formation of a passive film on the surface. Fig. 3 shows the XPS survey spectra for the passive film formed on UHSMSS in 0.1 M Na$_2$SO$_4$ solution (pH = 3) at OCP for 2 h. These results suggest that the passive film on UHSMSS surface is mainly composed of oxides and hydroxides of Fe, Cr, Ni, Mo, and Co. The alloying elements Mo and Co contribute to the formation of passive films. UHSMSS samples were also immersed in 0.1 M Na$_2$SO$_4$ solution (pH = 3) at 1.4 V$_{SCE}$ (above the pitting potential) for 5 min; the resulting surface morphology is shown in Fig. 2. In this case, pitting instead of passivation was observed on UHSMSS surface.

The AFM topography images in two-dimensional height and adhesion of the passive film formed on UHSMSS in 0.1 M Na$_2$SO$_4$ solution (pH = 3) at OCP for 2 h and the surface fresh steel etched with HF: HCl: H$_2$O = 4:4:92 solution are shown in Fig. 4, respectively.
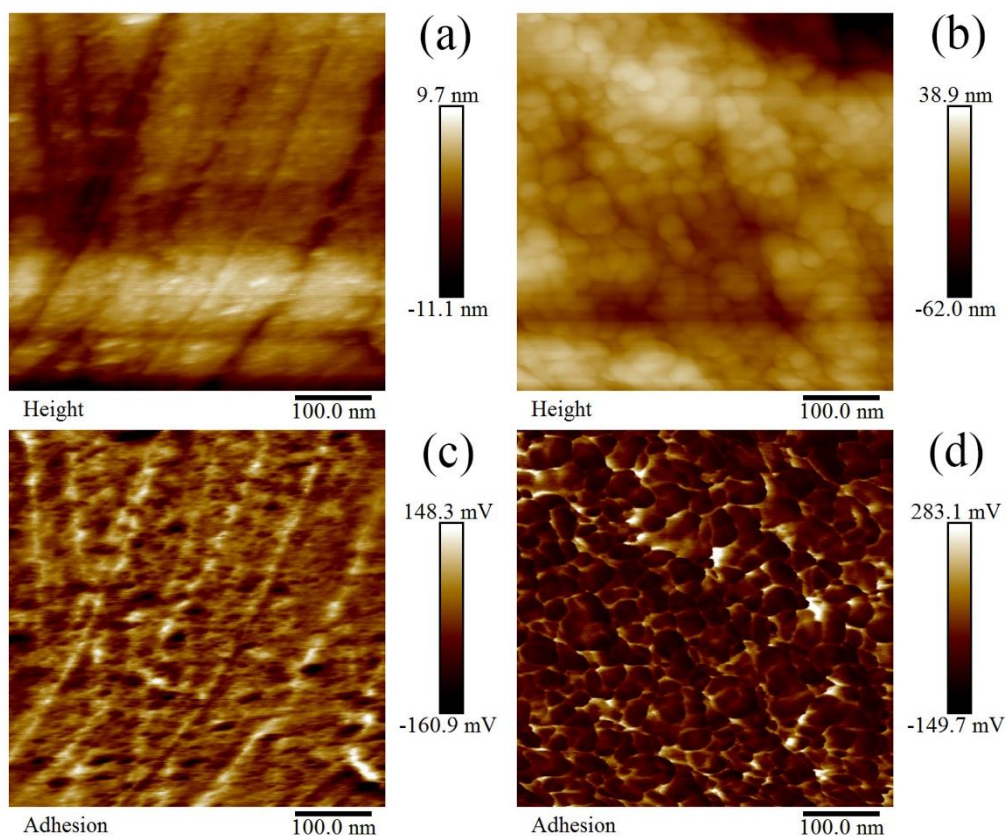
Figure 4. 2D AFM height and adhesion morphologies of the passive film on UHSMSS formed at OCP for 2 h (a, c) and the etched surface (b, d)

As shown in Fig. 4(a) and (b), the height of the surface passive film was much lower than that of the etched surface for the martensite; in addition, the grain boundaries reacted and dissolved under the effect of the erodent. Fig. 4(c) and (d) shows that the adhesion of the passive film was less than that of the matrix. The passive film was more uniform but less firmly adhered to the matrix than the matrix itself.

3.3 Structure of the passive film

To further investigate the electrochemical properties of the passive film of the UHSMSS, the samples were immersed in 0.1 M Na_2SO_4 solution (pH = 3) at -0.45 V_{SCE}, 0.1 V_{SCE}, 0.6 V_{SCE}, and OCP for 5 h to obtain a steady-state passive film to be measured. EIS is widely used to characterize the electrical properties of passive films. Before the EIS measurements were carried out, the passive films were formed on UHSMSS at 0.6 V_{SCE}, 0.1 V_{SCE}, -0.45 V_{SCE}, and OCP for 5 h, and the steady-state current density (I_{ss}) was recorded, as shown in Fig. 6(a). I_{ss} is clearly independent of the formation potential, which suggests that the surface conditions of the passive films formed at different potentials are stable but exhibit some differences.
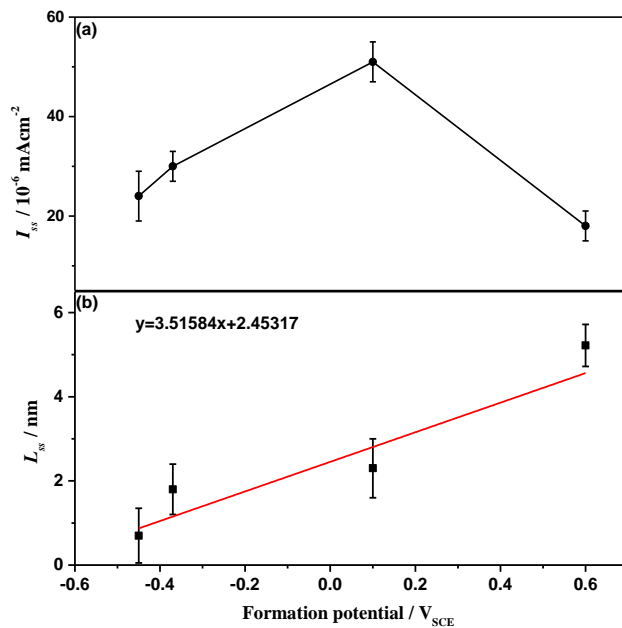
Figure 5. (a) Steady-state current density and (b) steady-state passive film thickness vs. the formation potential
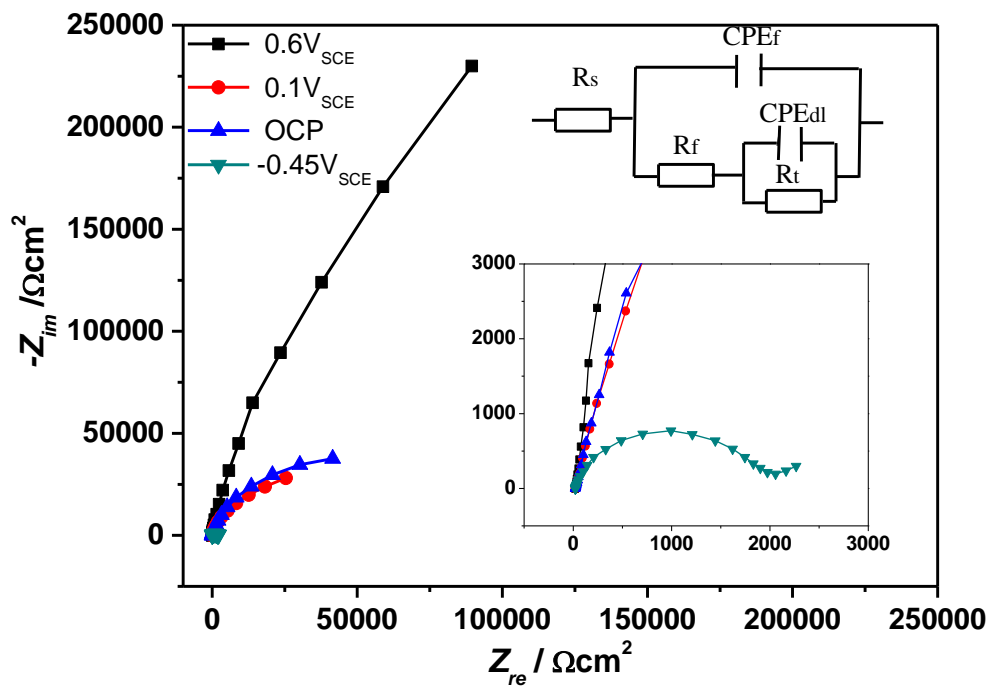
Figure 6. Nyquist diagrams of the passive films formed on the Cr12Ni3Co12Mo4W UHSMSS in 0.1 M Na_2SO_4 solution (pH = 3) at 0.6 V_{SCE}, 0.1 V_{SCE}, -0.45 V_{SCE}, and OCP for 2 h

The Nyquist diagrams of the passive films formed on UHSMSS in 0.1 M Na_2SO_4 solution (pH = 3) at different potentials are shown in Fig. 6. The radius of Nyquist diagrams increases as the passive film formation potential becomes more positive. The Nyquist plots were well fitted with the electrochemical equivalent circuits shown in the inset of Fig. 6, where R_s is the solution resistance, CPE_f is the double-charge-layer capacitance, R_f is the charge-transfer resistance, CPE_{dl} is the capacitance of the corrosion product formed on the electrode surface, and R_t is the resistance of the corrosion product. Numerous experiments on stainless steel have confirmed this equivalent circuit model, including experiments on 316L austenitic stainless steel in chlorine solution [22] and on Aermet100 ultra-high-strength steel in sulfuric acid solution [23].

Table 2. Values of fitting parameters observed from the Nyquist diagrams

	R_s /Ωcm^2	Q_f /$\Omega^{-1}s^n cm^{-2}$	n_1	R_f /Ωcm^2	Q_{dl} /$\Omega^{-1}s^n cm^{-2}$	n_2	R_t /Ωcm^2
0.6V	20.11	2.645×10^{-5}	0.9980	16.69	2.816×10^{-5}	0.8911	9.478×10^{-5}
0.1V	19.40	6.028×10^{-5}	0.9055	17.15	7.412×10^{-5}	0.8789	8.84×10^{-4}
OCP	19.25	7.660×10^{-5}	0.9437	14.54	1.480×10^{-4}	0.8581	5.85×10^{-4}
-0.45V	20.88	1.982×10^{-4}	0.8550	1974	3.643×10^{-5}	1	317.1

The fitting data for the equivalent circuit are listed in Table 2. The solution resistance R_s values under the four investigated conditions are approximately the same, which suggests that the test environment is stable. Parameter Q_f gradually increases with decreasing potential, indicating that the passive film is more defective.

The capacitance C of the passive film can be calculated by:

$$C = \frac{(QR)^{1/n}}{R} \quad (1)$$

where Q and R correspond to Q_f and R_f, respectively, n is equal to n_1. The thickness of the passive film can then be estimated by:

$$L_{ss} = \frac{\varepsilon\varepsilon_0 A}{C} \quad (2)$$

where ε is the dielectric constant of the passive film (taken as 15.6 [24]), ε_0 is the vacuum permittivity (8.854×10^{-14} F/cm), and A is the surface area. The relationships of formation potential and passive film thickness are shown in Fig. 5(b). The thicknesses of passive films are arranged from 0.7 nm to 5.2 nm as the formation potential is increased in the positive direction. The passive film thickness and the formation potential exhibit a linear relationship [25].

3.4 Electronic properties of the passive films

The Mott-Schottky test was used to further study the electronic properties of the passive films. The Mott-Schottky plots of the passive films formed on UHSMSS in 0.1 M Na_2SO_4 solution (pH = 3) at 0.6 V_{SCE}, 0.1 V_{SCE}, -0.45 V_{SCE}, and OCP are shown in Fig. 7. The slopes of the curves change at 0.6 V_{SCE}, 0.9 V_{SCE} and 1.1 V_{SCE}. The passive films exhibit n-type semiconductor behavior in the potential range from -0.1 V_{SCE} to 0.6 V_{SCE} (part I) and that from 0.9 V_{SCE} to 1.1 V_{SCE} (part III), as indicated by the positive slope. By contrast, the films exhibit p-type semiconductor behavior in the potential range from 0.6 V_{SCE} to 0.9 V_{SCE} (part II) and that from 1.1 V_{SCE} to 1.5 V_{SCE} (part IV), as indicated by the negative slope. The shift between n-type and p-type semiconductor behavior is likely caused by changes in the composition and structure of the passive films [26].
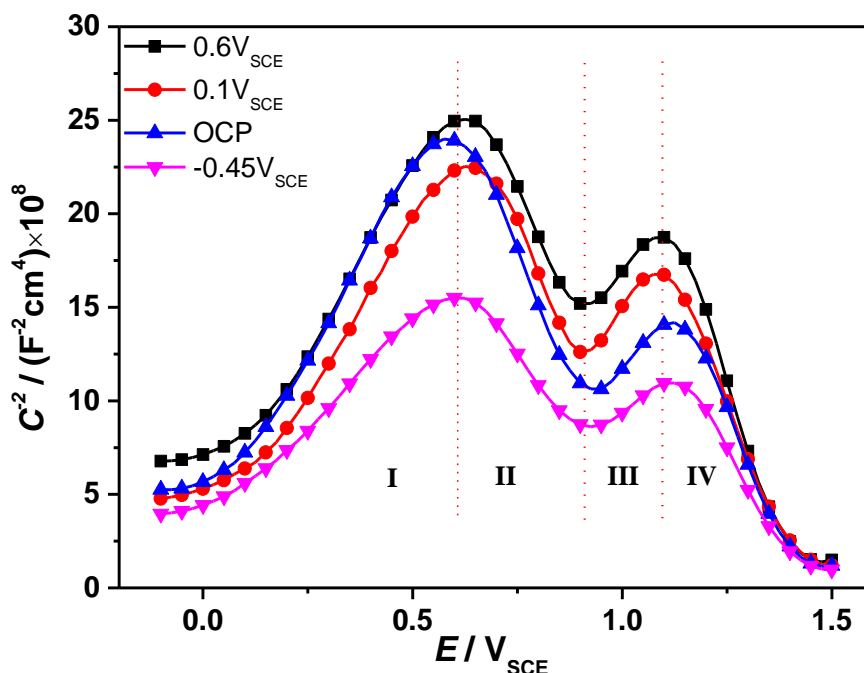

Figure 7. The Mott-Schottky plots of the capacitance behavior of the passive film formed on the Cr12Ni3Co12Mo4W UHSMSS in 0.1 M Na_2SO_4 solution (pH = 3) at -0.6 V_{SCE}, 0.1 V_{SCE}, -0.45 V_{SCE}, and OCP

The electronic properties of the four types of passive films formed at 0.6 V_{SCE}, 0.1 V_{SCE}, -0.45 V_{SCE}, and OCP exhibit obvious differences, as indicated by their Mott-Schottky curves. The donor density and acceptor density representing the electronic properties of the passive films are determined by the Mott-Schottky relationship, which describes the change in the space-charge layer capacitance (*C*) of the passive film as a function of applied potential (*E*):

$$\frac{1}{C^2} = \frac{2}{\varepsilon_0 e N_D}\left(E - E_{fb} - \frac{kT}{e}\right) \text{ n-type (3)}$$

$$\frac{1}{C^2} = \frac{-2}{\varepsilon_0 e N_A}\left(E - E_{fb} - \frac{kT}{e}\right) \text{ p-type (4)}$$

where ε is the dielectric constant of the passive film (taken as 15.6 [24]), ε_0 is the vacuum permittivity (8.85×10^{-14} F/cm), e is the electron charge (1.602×10^{-19} C), N_D is the donor density, N_A is the acceptor density, E_{fb} is the flat band potential, k is the Boltzmann constant (1.38×10^{-23} J/K), and T is the absolute temperature (the tests were conducted at 298K) [27-28].
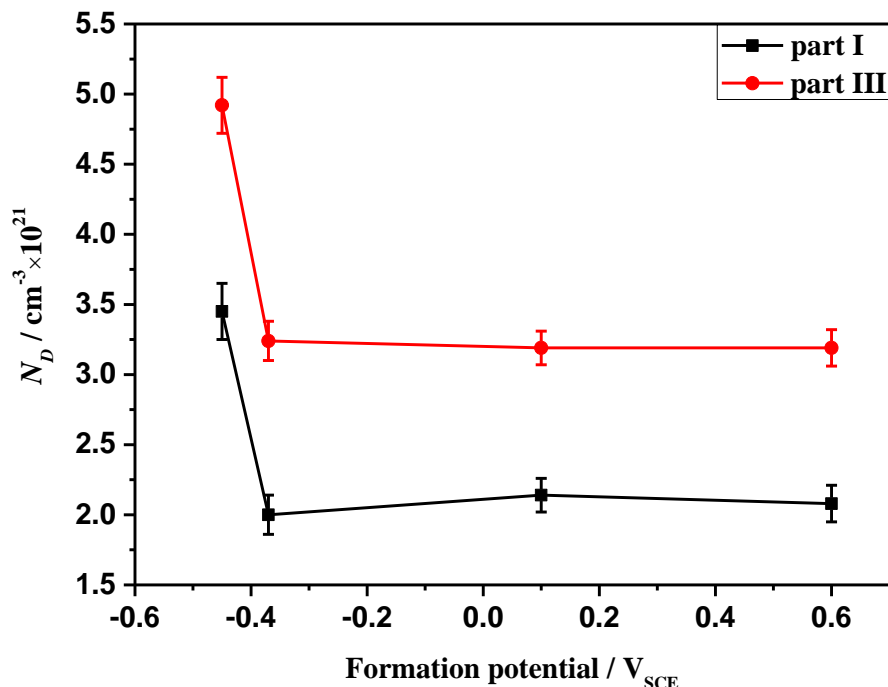

Figure 8. Donor concentration in the passive film formed on the Cr12Ni3Co12Mo4W UHSMSS in 0.1 M Na_2SO_4 solution (pH = 3) at different potentials

The n-type semiconductor behavior is attributable to oxygen vacancies and Cr^{3+} interstitials in the films. The donor density (N_D) was calculated from equation (3); the relationship between N_D and the formation potential is displayed in Fig. 8. N_D decreases quickly and becomes stable with increasing formation potential. The N_D value is larger when the passive film formation potential is in the cathodic region than at positive potentials because an unstable oxide layer is formed on UHSMSS surface in the cathodic region. Moreover, when the passive film formation potential is in the anodic region, N_D is small because a stable passive film is formed on the surface and the concentration of oxygen vacancies is decreased. According to the point defect model [29], oxygen vacancies in a passive film can absorb chloride ions, which lead to breakdown of the passive film. Thus, when the passive film formation potential is lower, the donor density is higher, and the passive film is easier to break down. This easier film breakdown is why the pitting susceptibility of a passive film is proportional to its donor density.

According to previous research on the semiconductor properties of passive films on stainless steels, oxides such as Fe_2O_3, MoO_3, and FeOOH exhibit n-type semiconductor behavior [25], whereas

Cr_2O_3, NiO, MoO_2, and $FeCr_2O_4$ exhibit p-type semiconductor behavior. The analysis of the XPS survey spectra of the passive films suggests that the passive films on the specimens are composed of oxides and hydroxides of Fe, Cr, Ni, Co, and Mo. Further study on the composition of the passive film formed on UHSMSS is critical.

3.5 Composition of the passive film
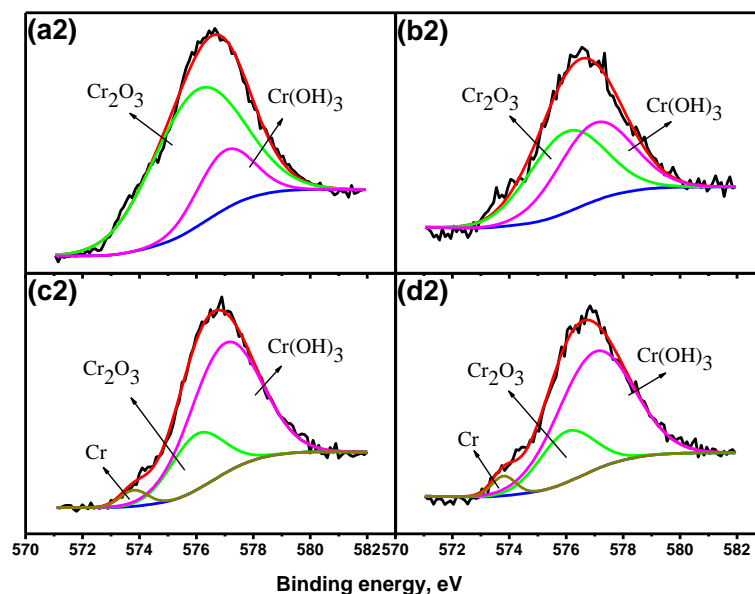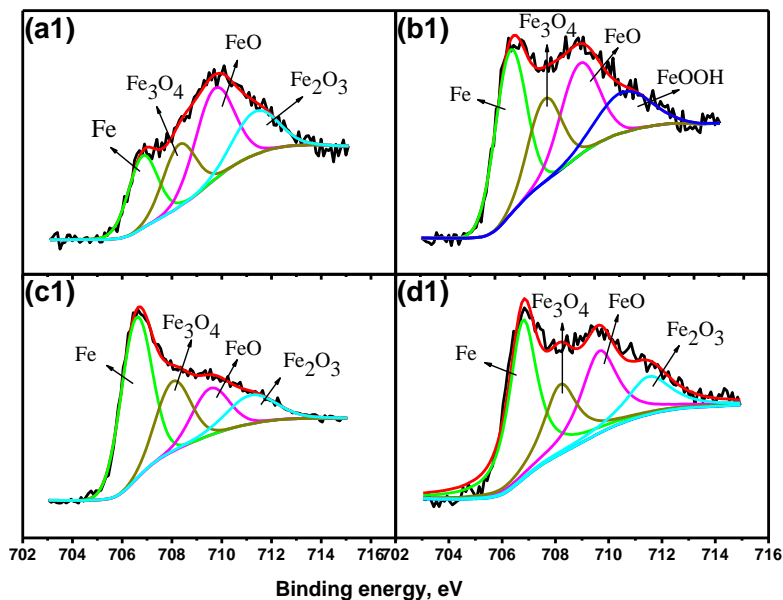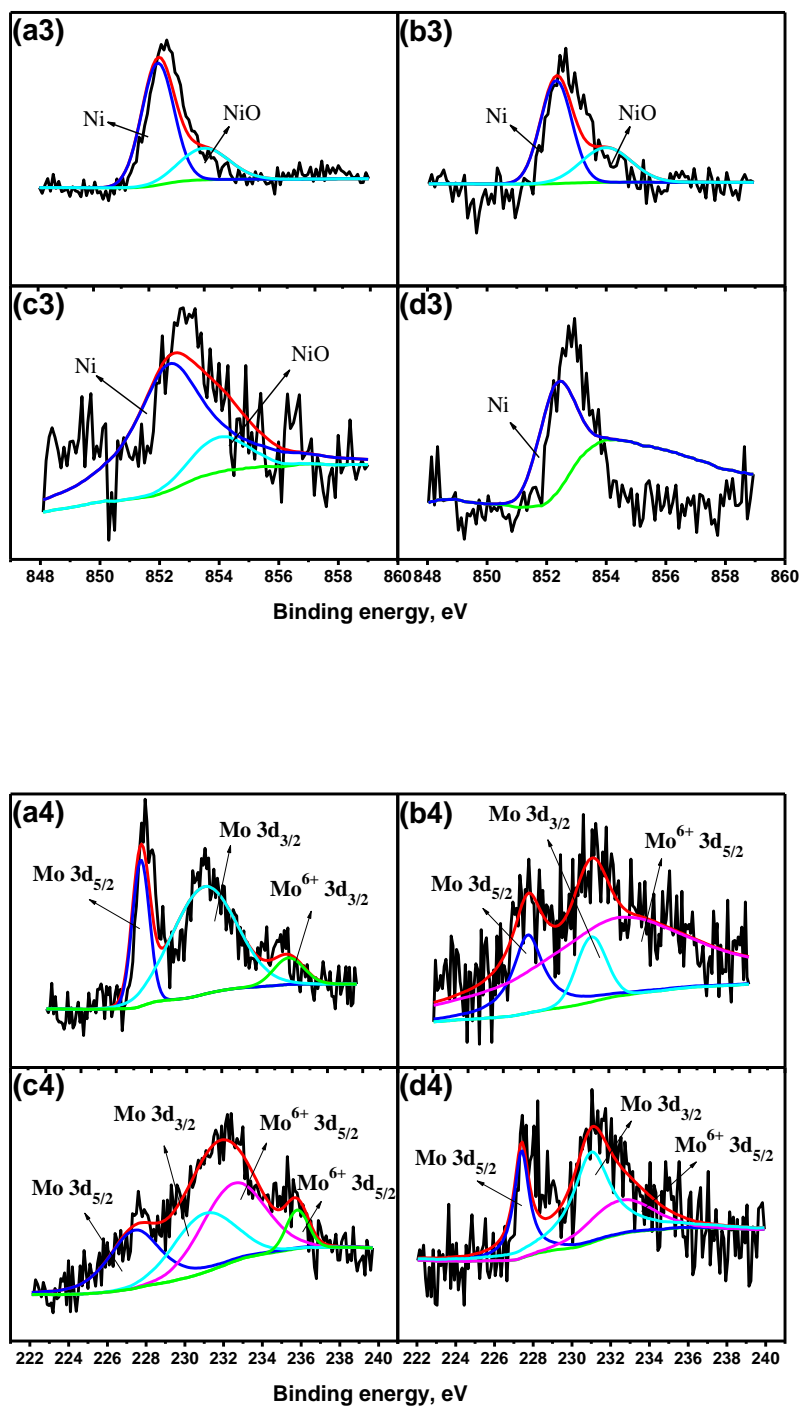
Figure 9. XPS spectra of Fe $2p_{3/2}$, Cr $2p_{3/2}$, Ni $2p_{3/2}$, Mo $3d_{5/2}$, and $3d_{3/2}$ of the passive film formed on Cr12Ni3Co12Mo4W UHSMSS in 0.1 M Na_2SO_4 solution (pH = 3) at (a) 0.6 V_{SCE}; (b) 0.1 V_{SCE}; (c) OCP and (d) -0.45 V_{SCE}

XPS analysis was carried out to characterize the composition of UHSMSS passive films formed in 0.1 M Na_2SO_4 solution (pH = 3) at different formation potentials. Fig. 9 presents the Fe $2p_{3/2}$, Cr $2p_{3/2}$, Ni $2p_{3/2}$, and Mo 3d XPS spectra collected from areas on the surface of the passive films.

After Shirley background subtraction, the XPS results were separated into contributions of the different oxidation states by a fitting procedure described elsewhere [30-33]. The spectra for the passive films formed at 0.6 V_{SCE} and 0.1 V_{SCE} indicate almost the same film composition, and the compositions of the passive films formed at OCP and at -0.45 V_{SCE} differ only slightly. The deconvolution and fitting of the spectra were performed on the basis of the corresponding binding energies published in the NIST atomic spectra database and in previous reports [34-35], as listed in Table 3.

Table 3. Binding energies of the primary passive film compounds formed on the Cr12Ni3Co12Mo4W UHSMSS obtained from the XPS spectra deconvolution

Element	Peak	Species / binding energy(eV)
Fe	$2p_{3/2}$	Fe / 706.5eV，FeO / 709.9eV，Fe_3O_4 / 708.2eV，Fe_2O_3 / 711.5eV，FeOOH / 712eV；
Cr	$2p_{3/2}$	Cr / 573.8eV，Cr_2O_3 / 576.0eV，$Cr(OH)_3$ / 577.0eV，CrO_3 / 578.3eV
Ni	$2p_{3/2}$	Ni / 852.32eV，NiO / 854eV，$Ni(OH)_2$ / 855.78eV
Mo	$3d_{5/2}$	Mo / 227.4eV; Mo^{4+} / 228.8eV; Mo^{6+} / 232.5eV
	$3d_{3/2}$	Mo / 231eV; Mo^{4+} / 234.2eV; Mo^{6+} / 235.8eV

Table 4. The atomic concentration of the passive films formed on the Cr12Ni3Co12Mo4W UHSMSS at different formation potentials obtained from the XPS spectra deconvolution

|	C 1s	O 1s	Cr 2p	Fe 2p	Ni 2p	Mo 3d
0.6 V_{SCE}	14.70	46.29	14.46	21.06	3.19	0.29
0.1 V_{SCE}	33.31	37.29	9.31	18.29	1.70	0.08
OCP	25.55	41.81	11.92	18.08	2.46	0.15
-0.45 V_{SCE}	26.45	49.61	12.78	10.33	0.77	0.05

The Fe 2p signals in Fig. 9 indicate the presence of Fe, Fe_3O_4, FeO, Fe_2O_3, and FeOOH. With increasing formation potential, the contents of Fe and FeO decrease, as indicated by the decrease in intensity of their associated peaks, whereas the content of Fe_2O_3 increases. It suggests that the Fe^{3+} is the primary oxidized iron species in the passive films. In the case of the Cr 2p spectra in Fig. 9, the oxides and hydroxides of Cr in the passive films primarily comprised Cr_2O_3 and $Cr(OH)_3$. The Cr_2O_3

content increases with increasing formation potential, while the $Cr(OH)_3$ content decreases. At lower formation potentials, a negligible Cr peak is observed. It indicates that the Cr_2O_3 is the most stable oxide species of Cr in the passive films.

The spectra of Ni 2p in Fig. 9 indicate the presence of Ni (852.32 eV) and NiO (854 eV). The preferential formation of NiO occurs at higher formation potentials; when the potential was decreased to -0.45 V_{SCE}, no NiO peak was observed. The Mo 3d spectra in Fig. 9 indicate the presence of metallic Mo and hexavalent Mo^{6+}; no peak associated with the unstable tetravalent Mo^{4+} was observed. Collectively, the XPS spectra suggest that the passive films on UHSMSS specimens are composed mainly of FeO, Fe_3O_4, Fe_2O_3, Cr_2O_3, $Cr(OH)_3$, NiO, and MoO_3. Extensive literature confirms that the passive films on stainless steels consist of an inner layer of Cr_2O_3 and an outer layer of Fe_3O_4 [22-23].

The atomic concentrations of the passive films formed on UHSMSS at different formation potentials, as obtained from deconvolution of the XPS spectra, are listed in Table 4. The Cr/Fe element ratio in the passive films formed at 0.6 V_{SCE}, 0.1 V_{SCE}, OCP, and -0.45 V_{SCE} are 0.69, 0.51, 0.66, and 1.24, respectively. Thus, the XPS results indicate that the passive films formed at anodic potentials are mainly composed of FeO, Fe_3O_4, and Fe_2O_3, whereas the passive films formed at cathodic potentials are mainly composed of Cr_2O_3 and $Cr(OH)_3$. The atomic concentration of Ni is greater than that of Mo, in contrast to their relative concentrations content in the substrate. It suggests that the contribution of the alloy element Ni to the passivation performance is greater than the contribution of Mo. This information is important from the viewpoint of material design.

3.6 Electrochemical properties of the passive films
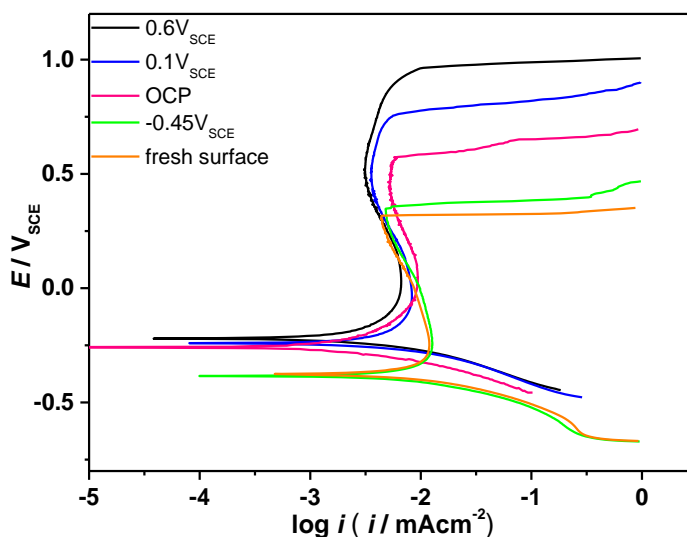
Figure 10. Polarization curves of the Cr12Ni3Co12Mo4W UHSMSS without and with passive films formed at 0.6 V_{SCE}, 0.1 V_{SCE}, OCP and -0.45 V_{SCE} in 0.5 M NaCl solution (pH = 3)

To further study the effect of passive films on the electrochemical behavior of the Cr12Ni3Co12Mo4W UHSMSS, we collected potentiodynamic polarization curves of UHSMSS

specimens with and without passive films. Fig. 10 shows the potentiodynamic polarization curves for UHSMSS without and with passive films formed at 0.6 V_{SCE}, 0.1 V_{SCE}, OCP, and -0.45 V_{SCE} in 0.5 M NaCl solution (pH = 3). The corrosion potentials of UHSMSS with passive films formed at 0.6 V_{SCE} and at 0.1 V_{SCE} are higher than that of specimen without passive films at OCP and -0.45 V_{SCE}. Compared with the polarization curve of the fresh surface, the corrosion potential and pitting potential of the UHSMSS specimens with passive films are more positive, which is similar with the results of other ultra high strength [36]. It indicates that the protection provided by the passive films on UHSMSS is enhanced with increasing formation potential.

As evident from the polarization curves in Fig. 10, when pitting occurred, the currents of the UHSMSSs with passive films formed at 0.6 V_{SCE} and 0.1 V_{SCE} slowly increased, indicating that the passive films slowly dissolved before pitting occurred. However, the currents of UHSMSS specimens without and with passive films formed at OCP and -0.45 V_{SCE} sharply increased, consistent with the presence of thin passive films that rapidly dissolved.

4. CONCLUSIONS

In the present work, the passivation properties of the Cr12Ni3Co12Mo4W UHSMSS were investigated by XPS, AFM, and a series of electrochemical measurements. The thickness, structure and composition of the passive films formed on the surface of UHSMSS specimens at different potentials were studied. The effect of the passive films on the electrochemical behavior of UHSMSS specimens is evaluated. The main conclusions obtained from this work are summarized as follows:

(1) The Cr12Ni3Co12Mo4W UHSMSS exhibited excellent passivation properties in 0.1 M Na_2SO_4 solution (pH = 3) by forming a passive film on their surface. The thickness of the passive film showed a linear relationship with the formation potential, which increased from 0.7 nm to 5.2 nm when the film formation potential was increased from -0.45 V_{SCE} to 0.6 V_{SCE}.

(2) The passive films formed at different potentials performed n-type and p-type semiconductor behavior. The donor density decreased quickly and then became stable with increasing formation potential. The passive films formed at higher potentials were more stable than those formed at lower potentials.

(3) The passive films formed on the Cr12Ni3Co12Mo4W UHSMSS were composed mainly of FeO, Fe_3O_4, Fe_2O_3, Cr_2O_3, $Cr(OH)_3$, NiO, and MoO_3. The passive films formed at anodic potentials primarily comprised Fe oxides, whereas those formed at cathodic potentials contained primarily oxides and hydroxides of Cr.

(4) UHSMSS exhibited excellent pitting corrosion resistance in 0.5 M NaCl solution (pH = 3). The passive films formed at passivation potentials protected UHSMSS from pitting, and the protection was enhanced with increasing passivation potential.

References

1. D. Figueroa and M. Robinson, *Corros. Sci.* 52 (2010) 1593.
2. D. Figueroa and M. Robinson, *Corros. Sci.* 50 (2008) 1066.
3. L. Tsay, M. Chi, Y. Wu, J. Wu and D. Lin, *Corros. Sci.* 48 (2006) 1926.
4. J. Petit, C. Sarrazin-Baudoux and F. Lorenzi, *Proc. Eng.* 2 (2010) 2317.
5. Q. Guo, J. Liu, M. Yu and S. Li, *Appl. Surf. Sci.* 327 (2015) 313.
6. A. Abad, M. Hahn and O. Es-Said, *Eng. Fail. Anal.* 17 (2010) 208.
7. A. Mondelin, F. Valiorgue, J. Rech, M. Coret and E. Feulvarch, *Int. J. Mech. Sci.* 58 (2012) 69.
8. A. Jha, K. Sreekumar and P. Sinha, *Eng. Fail. Anal.* 17 (2010) 1195.
9. V. Vignal, H. Zhang, O. Delrue, O. Heintz, I. Popa and J. Peultier, *Corros. Sci.* 53 (2011) 894.
10. S. Haleem, E. Aal, S. Wanees and A. Diab, *Corros. Sci.* 52 (2010) 3875.
11. B. Diaz, L. Freire, X. Novoa and M. Perez, *Electrochim. Acta* 54 (2009) 5190.
12. Y. Qiao, Y. Zheng, W. Ke and P. Okafor, *Corros. Sci.* 51 (2009) 979.
13. Y. Zhang, M. Urquidi-Macdonald, G. Engelhardt and D. Macdonald, *Electrochim. Acta* 69 (2012) 1.
14. T. Shibata and Y. Zhu, *Corros. Sci.* 37 (1995) 253.
15. M. Serdar, L. Zulj and D. Bjegovic, *Corros. Sci.* 69 (2013) 149.
16. R. Jung, H. Tsuchiya, S. Fujimoto, *Corros. Sci.* 58 (2012) 62.
17. C. Olsson and D. Landolt, *Electrochim. Acta* 48 (2003) 1093.
18. Y. Zhang, M. Urquidi-Macdonald, G. Engelhardt and D. Macdonald, *Electrochim. Acta* 69 (2012) 12.
19. Y. Zhang, M. Urquidi-Macdonald, G. Engelhardt, and D. Macdonald, Electrochim. Acta 69 (2012) 19.
20. M. Sun, K. Xiao, C. Dong, X. Li and P. Zhong, *Aerosp. Sci. Technol.* 36 (2014) 125.
21. M. Sun, K. Xiao, C. Dong, X. Li and P. Zhong, *Corros. Sci.* 89 (2014) 137.
22. Y. Hu, C. Dong, M. Sun, K. Xiao, P. Zhong and X. Li, *Corros. Sci.* 53 (2011) 4159.
23. J. Ding, L. Zhang, M. Lu, J. Wang, Z. Wen and W. Hao, *Appl. Surf. Sci.* 289 (2014) 33.
24. A. Pada, D. Shukla and U. Stimming, *Electrochim. Acta* 36 (1991) 345.
25. S. Gao, C. Dong, X. Cheng, K. Xiao, L. Wang and X. Li, *Corrosion* 70 (2014) 627.
26. Z. Feng, X. Cheng, C. Dong, L. Xu and X. Li, *Corros. Sci.* 52 (2010) 3646.
27. W. Li and J. Luo, *Electrochem. Commun.* 1 (1999) 349.
28. W. Li and J. Luo, *Int. J. Electrochem. Sci.* 2 (2007) 627.
29. D. Macdonald, *J. Electrochem. Soc.* 139 (1992) 3434.
30. C. Donik, A. Kocijan, J. Grant, M. Jenko, A. Drenik and B. Pihlar, *Corros. Sci.* 51 (2009) 827.
31. H. Luo, C. Dong, K. Xiao and X. Li, *Appl. Surf. Sci.* 258 (2011) 631.
32. C. Liu and J. Wu, *Corros. Sci.* 49 (2007) 2198.
33. D. Shirley, *Phys. Rev. B* 5 (1972) 4709.
34. L. Guo, M. Lin, L. Qiao and A. Volinsky, *Corros. Sci.* 78 (2014) 55.
35. D. Li, *Ultrason. Sonochem.* 27 (2015) 296.
36. H. Li, C. Dong, K. Xiao, X. Li and P. Zhong, *Int. J. Electrochem. Sc.* 10 (2015) 10173.